Iron-Loss and Magnetic Hysteresis Under Arbitrary Waveforms in NO Electrical Steel: A Comparative Study of Hysteresis Models

Simon Steentjes, Kay Hameyer, *Senior Member, IEEE*, Drago Dolinar, *Member, IEEE*, and Martin Petrun, *Member, IEEE*

***Abstract*—This paper presents a comparative study of different static hysteresis models coupled to the parametric magneto-dynamic model of soft magnetic steel sheets. Both mathematical and behavioral as well as physically based approaches are discussed with respect to the ability to predict the dynamic hysteresis loop shape and iron loss under arbitrary excitation waveforms. Both current- as well as voltage-driven excitation cases are evaluated. The presented analysis discusses and points out advantages and limitations of the majority of the well-known static hysteresis models. In this way, it supports the selection of adequate hysteresis models for the specific application, i.e., smooth excitations, distorted flux waveforms, transients, or steady-state regimes. Comparisons against measurements for a *M400-50A* electrical steel over a wide range of magnetic flux density and frequencies for both sinusoidal and arbitrary excitations are analyzed. In the analysis hysteresis loop shapes, power losses as well as NRMS errors of individual loop sections are compared.**

***Index Terms*—Eddy currents, iron losses, magnetic hysteresis, magnetization dynamics, pulse width modulation (PWM), soft magnetic materials.**

I. Introduction

THE prediction of the magnetic behavior of soft magnetic steel laminations under arbitrary excitation waveforms is critical for the design and further improvement of electromagnetic energy transducers. Particularly crucial is the prediction of iron loss and dynamic magnetization during the operation of rotating electrical machines [1]–[5] or energy converters, such as, e.g., dc–dc converters [6], [7] that operate under pulse width modulation (PWM)-like excitations. Nevertheless material data (iron loss and magnetization curves) supplied by the data sheet or acquired through standardized measurements under sinusoidal magnetic flux density waveform do not apply for the magnetic components of inverter driven electrical energy converters and rotating electrical machines.

For instance, PWM-like voltage waveforms occurring in dc–dc converters [6], [7] significantly affect and exacerbate the iron-loss prediction based on standardized measured data. Among others, the PWM inverter characteristics such as the modulation index or pulse wave affect the iron loss which are directly related to the hysteresis loop shape.

Useful engineering methodologies for iron-loss predictions in magnetic laminations supplied with a PWM waveform either require a large amount of measured data for parameter identification or are prone to large prediction errors [8]–[11]. They do not account for the complex interplay between magnetic hysteresis and eddy currents in the laminations [11]–[13].

In order to accurately predict the iron-loss and magnetization behavior of non-oriented (NO) soft magnetic steel sheets (SMSS) under arbitrary excitation waveforms, it is indispensable to utilize a hysteresis model directly coupled to an eddy-current (lamination) model [14]–[19].

Conventional hysteresis models such as Preisach or Jiles-Atherton (J-A) address hysteresis effects independently of the eddy currents. In this paper, a strongly coupled model that addresses both phenomena simultaneously is developed in such a way that the interplay between skin effect, i.e., eddy currents across laminations and hysteresis can be resolved accurately.

With the help of the parametric magneto-dynamic (PMD) model [19]–[22], the magnetization processes in thin and long SMSSs neglecting edge effects is described. This model offers the flexibility to implement various inverse hysteresis models to analyze their ability to handle the intricate problem. The applied hysteresis model utilized to represent the constitutive relation of the SMSS is critical for the resulting eddy-current and flux distributions due to different magnetization trajectories in various layers of the sheet.

The aim of this paper is to present a direct comparative analysis of most of the well-known static hysteresis models in combination with the PMD model for the prediction of magnetization dynamics under arbitrary excitation waveforms, i.e., PWM-like excitation. Both purely mathematical as well as phenomenological and physically based hysteresis models are studied. The

Manuscript received January 4, 2016; revised March 19, 2016; accepted March 31, 2016. Date of publication May 18, 2016; date of current version February 9, 2017. This work was supported in part by ARRS, Project Number P2-0115. The work of S. Steentjes was supported by the DFG and carried out in the research project "Improved modeling and characterization of ferromagnetic materials and their losses."

S. Steentjes and K. Hameyer are with the Institute of Electrical Machines, RWTH Aachen University, D-52062 Aachen, Germany (e-mail: simon.steentjes@iem.rwth-aachen.de; kay.hameyer@iem.rwth-aachen.de).

M. Petrun and D. Dolinar are with the Institute of Power Engineering, FERI, University of Maribor, SI-2000 Maribor, Slovenia (e-mail: martin.petrun@um.si; drago.dolinar@um.si).

Color versions of one or more of the figures in this paper are available online at http://ieeexplore.ieee.org.

Digital Object Identifier 10.1109/TIE.2016.2570200

only constraint here is the contemplation of history-independent hysteresis models.

II. PMD Model

The spatially random domain structure and the small grain size of NO soft magnetic materials allow to treat these properties as homogeneous isotropic. In this case, the magnetization dynamics can be described by the classical Maxwell equations where eddy currents are assumed to flow parallel to the surface of the sheet and domain dynamics are neglected [17].

In the case of a thin steel strip, the one-dimensional penetration equation (1) describes the diffusion phenomena with adequate accuracy [19]. Therefore, the magnetization dynamics, induced eddy currents as well as the distribution of the magnetic field and consequently the shape of the dynamic hysteresis loop can be determined

$$\sigma \frac{\partial B}{\partial t} = \frac{\partial^2 H}{\partial z^2}. \tag{1}$$

The static hysteresis model used to describe the static magnetization behavior in (1) is crucial for the accuracy, computational performance and resulting magnetic field, and flux distribution. Therefore, an in-depth study is required (see Section III).

In this paper, the PMD model of SMSSs [19]–[22] is used to solve the one-dimensional diffusion problem. The PMD model enables effortless implementation of different inverse static hysteresis descriptions.

The PMD model discretizes the magnetic field distribution inside a SMSS piece-wise uniformly across the sheet thickness by dividing the sheet into N_s equally thick slices. The magnetic field inside individual slices can be treated as uniform when the sheet is divided into an adequate number of slices [20]. The magnetic field inside the sheet is described by a system of differential equations for all slices. Based on average values and Faraday's law, the induced eddy currents i_es inside all the slices can be calculated. These affect the excitation of magnetic field inside individual slices directly. Considering this by expressing the equilibriums of magneto-motive forces (mmfs) in all the slices of the SMSS using Ampere's law, the PMD model is expressed by a simple system of ordinary differential equations (ODEs) (2) [19]–[22]

$$\boldsymbol{\Theta} = \mathbf{N} i_\mathrm{p} = \bar{\mathbf{H}}(\bar{\boldsymbol{\Phi}}) l_\mathrm{m} + \mathbf{L}_\mathrm{m} \frac{\mathrm{d}\bar{\boldsymbol{\Phi}}}{\mathrm{d}t} = \mathbf{R}_\mathrm{m} \bar{\boldsymbol{\Phi}} + \mathbf{L}_\mathrm{m} \frac{\mathrm{d}\bar{\boldsymbol{\Phi}}}{\mathrm{d}t}. \tag{2}$$

In (2), $\boldsymbol{\Theta}$ represents a vector of the mmf generated by the applied current i_p in the excitation winding, $\bar{\mathbf{H}}(\bar{\boldsymbol{\Phi}})$ is a vector of average magnetic field strengths as hysteretic functions of the average magnetic fluxes in the slices and l_m is the magnetic path length. $\mathbf{N}$ is a vector with the number of turns N of the excitation winding, $\mathbf{R}_\mathrm{m}$ is a vector of nonlinear reluctances and $\mathbf{L}_\mathrm{m}$ is the magnetic inductance matrix of the SMSS [20]–[22].

The presented PMD model can be both current and voltage driven, i.e., the magnetization dynamics can be calculated either based on the excitation current i_p using (2), or based on the applied voltage u_p to the excitation winding. For the voltage-driven excitation, the PMD model is extended by a model of the excitation winding (3), where u_p and u_i represent the applied and induced voltage in the winding and R_p and $L_{\sigma\mathrm{p}}$ represent the resistance and leakage inductance of the excitation winding, respectively,

$$u_\mathrm{p} = R_\mathrm{p} i_\mathrm{p} + L_{\sigma\mathrm{p}} \frac{\mathrm{d}i_\mathrm{p}}{\mathrm{d}t} + \underbrace{\mathbf{N}^\mathrm{T} \frac{\mathrm{d}\bar{\boldsymbol{\Phi}}}{\mathrm{d}t}}_{u_\mathrm{i}}. \tag{3}$$

The size of the obtained ODE system depends on the numerical discretization of the observed SMSS, i.e., the number of slices N_s. In case that only one slice is defined ($N_\mathrm{s} = 1$), the PMD model converges to the classical low-frequency eddy current approximation [19].

In order to study the magnetization dynamics in magnetically anisotropic grain-oriented materials, it is indispensable to introduce a time delay of the local magnetic flux density with respect to the magnetic field in all the slices of the sheet [17]. This could be effectively achieved using a magnetic viscosity in addition to the static hysteresis model. This paper is restricted to NO SMSSs obeying a fine and highly irregular domain structure where the diffusion equation (1) provides a fairly reliable basis for the computation of the dynamic hysteresis loops [17].

III. Hysteresis Models

The development of hysteresis models is influenced by generally conflicting demands regarding accuracy, simplicity, and physical behavior. The major driving forces are the ability to describe the shape of the static hysteresis loops and determine related energy loss.

Initially, magnetic hysteresis loops were modeled using mathematical models, e.g., the Preisach model [23] and its descendants or the Stop and Play models [24], [25]. These models are not closely related to the physics of the magnetic materials, and instead rely on empirical techniques involving the identification of parameters. Later on, physically-based models such as the energy-based hysteresis models involving a population of pseudo particles with friction-like pinning [16], [26], [27] or the quasi-mesoscopic model that minimizes the total energy to derive a fictitious reversible and irreversible magnetic field component [28] were developed.

Likewise, the field-separation principle advanced in [29] resembles the aforementioned descriptions of magnetic hysteresis effect. Those energy-based descriptions obtain the hysteresis loop branches by the introduction of an offset along the H-axis. These models are consistent with the laws of irreversible thermodynamics making those hysteresis models particularly interesting for engineers who need reliable hysteresis models based on sound physical grounds.

One of the most cited and used model is the J-A model [30], [31]. This model has been largely employed due to some advantages such as the relatively small number of parameters and the good computational performance. However, for the J-A model, there are still shortcomings with the identification of the model's parameter and its stability [32]. Particularly when modeling distorted and irregular hysteresis loops, the deviation between modeled and measured loops is often not adequate.

The GRUCAD model relies in contrast to the J-A model on the decomposition of total field strength into reversible and

irreversible terms [29] and could be easily extended in order to include other energy contributions.

Alternatively, transplantation type hysteresis models directly based on measured major loops or first-order reversal curves are suited for particular applications. In this respect, the simplest model is the Tellinen (TLN) model [33], where more advanced models represent the Zirka-Moroz (Z-M) hysteresis models [14].

The application of individual models depends on the complexity, accuracy, and other properties. The inverse $[H(B)]$ formulations are used due to the straightforward implementation in the PMD model of the SMSS.

A. J-A Hysteresis Model

The main equation of the inverse J-A hysteresis model [31] suitable for direct time dependence integration is given by

$$\frac{\mathrm{d}M}{\mathrm{d}B} = \frac{\delta_\mathrm{M}\left(M_\mathrm{an} - M\right) + \delta\, c\, k\, \frac{\mathrm{d}M_\mathrm{an}}{\mathrm{d}H_\mathrm{e}}}{\mu_0\left(\delta k + (1-\alpha)\left[\delta_\mathrm{M}\left(M_\mathrm{an} - M\right) + \delta\, c\, k\, \frac{\mathrm{d}M_\mathrm{an}}{\mathrm{d}H_\mathrm{e}}\right]\right)} \tag{4}$$

where the complementary relationships (5)–(9) apply. M_an is the anhysteretic magnetization that is described using the Langevin function $\mathrm{L}(x)$ by (5),

$$M_\mathrm{an} = M_\mathrm{s}\mathrm{L}\left(\frac{H_\mathrm{e}}{a}\right) = M_\mathrm{s}\left[\coth\frac{H_\mathrm{e}}{a} - \frac{a}{H_\mathrm{e}}\right]. \tag{5}$$

where H_e is the effective magnetic field (6)

$$H_\mathrm{e} = H + \alpha M. \tag{6}$$

The term $\frac{\mathrm{d}M_\mathrm{an}}{\mathrm{d}H_\mathrm{e}}$ in (4) is obtained by deriving (5) with respect to the effective field H_e using the derivative of the Langevin function $\mathrm{L}'(x)$ by

$$\frac{\mathrm{d}M_\mathrm{an}}{\mathrm{d}H_\mathrm{e}} = \frac{M_\mathrm{s}}{a}\mathrm{L}'\left(\frac{H_\mathrm{e}}{a}\right) = \frac{M_\mathrm{s}}{a}\left[1 - \coth^2\frac{H_\mathrm{e}}{a} + \left(\frac{a}{H_\mathrm{e}}\right)^2\right] \tag{7}$$

In (4)–(6), α, a, M_s, c, and k represent the J-A model parameters, whereas δ is the directional variable that corresponds to the sign of the derivative $\frac{\mathrm{d}B}{\mathrm{d}t}$.

As there is no domain wall displacement after a field reversal that caused negative $\frac{\mathrm{d}M}{\mathrm{d}H}$ slopes in the original J-A description, an additional control variable δ_M in (4) is introduced by

$$\delta_\mathrm{M} = \frac{1}{2} + \frac{1}{2}\mathrm{sign}\left[\left(M_\mathrm{an} - M\right)\frac{\mathrm{d}B}{\mathrm{d}t}\right]. \tag{8}$$

The output of the J-A model is the magnetic field strength H, which can be obtained using time integration of

$$\frac{\mathrm{d}H}{\mathrm{d}t} = \frac{1}{\mu_0}\frac{\mathrm{d}B}{\mathrm{d}t} - \frac{\mathrm{d}M}{\mathrm{d}t}. \tag{9}$$

B. GRUCAD Hysteresis Model

The concept of anhysteretic curve (truly reversible in the thermodynamic sense) is present in the hysteresis model proposed by the GRUCAD group [29]. The total field strength H is calculated from the integration of the sum of anhysteretic magnetic field H_an and hysteretic magnetic field H_h components using (10). Thereby, the source of problems originating in the assumption that total magnetization could be split into the reversible and the irreversible component is bypassed

$$\frac{\mathrm{d}H}{\mathrm{d}t} = \frac{\mathrm{d}H_\mathrm{an}}{\mathrm{d}t} + \frac{\mathrm{d}H_\mathrm{h}}{\mathrm{d}t}. \tag{10}$$

In order to obtain a system of ODE for direct time-dependent integration, H_an is determined by solving

$$\frac{\mathrm{d}H_\mathrm{an}}{\mathrm{d}B} = \frac{a_\mathrm{an} - \alpha_\mathrm{an} M_\mathrm{ans}\mathrm{L}'\left(\lambda_\mathrm{an}\right)}{\mu_0\left[a_\mathrm{an} + M_\mathrm{ans}\left(1-\alpha_\mathrm{an}\right)\mathrm{L}'\left(\lambda_\mathrm{an}\right)\right]} \tag{11}$$

where λ_an is defined by (12) and α_an, a_an, and M_ans represent the anhysteretic field component model parameters

$$\lambda_\mathrm{an} = \frac{1}{a_\mathrm{an}}\left[\left(1-\alpha_\mathrm{an}\right)H_\mathrm{an} + \alpha_\mathrm{an}\frac{B}{\mu_0}\right]. \tag{12}$$

The ODE representing the static hysteresis component of the field is given by (13)

$$\frac{\mathrm{d}H_\mathrm{h}}{\mathrm{d}B} = \frac{H_\mathrm{hs}\mathrm{L}\left(\lambda_\mathrm{h}\right) - H_\mathrm{h}}{\delta\gamma_\mathrm{h}} \tag{13}$$

where λ_h is defined by (14) and γ_h, a_h, and H_hs represent the hysteretic field component model parameters. The control variable δ as well as functions L and L′ are analogous to the J-A model description

$$\lambda_\mathrm{h} = \frac{1}{a_\mathrm{h}}\left[H_\mathrm{h} + \delta H_\mathrm{hs}\right]. \tag{14}$$

C. Stop Hysteresis Model

The Stop hysteresis model is based on the Stop hysteron [24], [25]. The scalar Stop model in the discretized form describes a hysteretic relation $H(B)$ by

$$H(B) = \sum_{\mathrm{m}=1}^{N_\mathrm{h}} g_\mathrm{m}\left(s_\mathrm{m}\left(B\right)\right) \tag{15}$$

where N_h is the number of hysteron operators, s_m is the mth Stop hysteron operator and g_m is the mth shape function $(m = 1, \ldots, N_\mathrm{h})$ of the model.

Stop operators are defined by (16), where B^0 and s_m^0 are the values of B and s_m at the previous moment in time, respectively, and η_m is a constant,

$$s_\mathrm{m}\left(B\right) = \max\left[\min\left(B - B^0 + s_\mathrm{m}^0, \eta_\mathrm{m}\right), -\eta_\mathrm{m}\right]. \tag{16}$$

In general, different shape functions can be applied for an adequate hysteresis description. In this paper, piece-wise linear (PWL) shape functions are assumed, with the constants set to $\eta_\mathrm{m} = \frac{mB_\mathrm{s}}{N_\mathrm{h}}$ [25]. A section of the PWL shape function g_m between two consecutive break points $s_{m,j-1}$ and $s_{m,j}$ $(s_{m,j-1} \le s \le s_{m,j})$ is defined by

$$g_\mathrm{m}\left(s\right) = g_\mathrm{m}\left(s_{m,j-1}\right) + \kappa_{m,j}\left(s - s_{m,j-1}\right) \tag{17}$$

where the mth PWL shape function has m break points $(j = 1, \ldots, m)$ that are defined by

$$s_{m,j} = -\eta_\mathrm{m} + j\Delta s = -\eta_\mathrm{m} + j\frac{2B_\mathrm{s}}{N_\mathrm{h}} \tag{18}$$

and $\kappa_{m,j} = \left[g_\mathrm{m}\left(s_{m,j}\right) - g_\mathrm{m}\left(s_{m,j-1}\right)\right]/\Delta s$ represent the slope of jth shape function section.

As the PWL shape functions are symmetric in respect to the origin, the starting value $g_{\mathrm{m}}\,(s_{m,0})$ of the first section of the shape function is defined by $g_{\mathrm{m}}\,(s_{m,0}) = -g_{\mathrm{m}}\,(s_{m,m})$.

D. TLN Hysteresis Model

The TLN model [33] is based on the major (limit) hysteresis loop, where $B^{+}_{\mathrm{lim}} = f(H)$ and $B^{-}_{\mathrm{lim}} = f(H)$ represent nonlinear functions or lookup table datasets that adequately describe the ascending and descending branches of the limit hysteresis loop as a function of H. The corresponding slopes of these functions $\mu^{+}_{\mathrm{lim}} = f(H)$ and $\mu^{-}_{\mathrm{lim}} = f(H)$ describe the permeability of both discussed branches.

Based on the material relations, the TLN model is expressed in form of two ODEs

$$\frac{\mathrm{d}H}{\mathrm{d}B} = \left[\mu_0 + \left(\mu^{+}_{\mathrm{lim}} - \mu_0\right)\frac{B^{-}_{\mathrm{lim}} - B}{B^{-}_{\mathrm{lim}} - B^{+}_{\mathrm{lim}}}\right]^{-1} \tag{19}$$

$$\frac{\mathrm{d}H}{\mathrm{d}B} = \left[\mu_0 + \left(\mu^{-}_{\mathrm{lim}} - \mu_0\right)\frac{B - B^{+}_{\mathrm{lim}}}{B^{-}_{\mathrm{lim}} - B^{+}_{\mathrm{lim}}}\right]^{-1} \tag{20}$$

where (19) is used when $\frac{\mathrm{d}B}{\mathrm{d}t} > 0 \;\; (\delta = 1)$ and (20) is used when $\frac{\mathrm{d}B}{\mathrm{d}t} < 0 \;\; (\delta = -1)$.

E. Z-M Hysteresis Model

The trajectories of the aforementioned hysteresis model are limited by the mathematical and physical constraints and are subsequently not applicable to all types of hysteretic behavior such as, e.g., wasp-waisted hysteresis loops. Alternatively, Z-M proposed to use a behavioral ("equation-free") hysteresis model, where, based on the major hysteresis loop, reversal curves of arbitrary order are constructed [14]. Central to the transplantation model is the assumption of a similarity between the trajectories of major and minor hysteresis loops. The history-dependent version intrinsically offers the correct construction of the major loop and ensures the most relevant empirical rules of Madelung such as the wiping-out property and the return-point memory [14].

In this paper, the Z-M history-independent model is employed [14], which does not retain any information about the magnetization history and constructs all internal loops based on the major loop data, i.e., all reversal curves of any order merge at the major loop tip. Central to this Z-M model is the gap ΔH between the major loop trajectory, i.e., ascending or descending branch, and the reversal curve at the level B_{p}

$$\Delta H(x) = \Delta H_R (1-b) x e^{-a(1-x)} + \tau \Delta H_{\mathrm{out}}(B_{\mathrm{p}}) b x^{c} \tag{21}$$

where ΔH_{out} is the width of the major loop, τ a scaling factor, and ΔH_R the field distance of the reversal point to the right branch of the major loop. a, b, c are constants calculated using (22), (23) and x is the dimensionless quantity specifying the ratio of the distance of the loop tip from the current level and the distance of the reversal point to the loop tip, which is decreasing from 1 to 0

$$a = \Delta B_{\mathrm{rev}}(7.73 + 2.76\beta - 28.63\beta^2 + 28.36\beta^3) \tag{22}$$

$$b = 0.22(1-\beta), \quad c = 0.125. \tag{23}$$

ΔB_{rev} is the distance from the reversal point to the major loop tip and β the dimensionless ratio of ΔB_{rev} and the height of the major loop [14].

IV. Implementation and Parameter Identification

For this comparison, the current- and voltage-driven PMD model versions are implemented using MATLAB/Simulink software. Different versions of the PMD model by applying the discussed hysteresis models are evaluated and compared, where experimental data (measured voltages and currents) are used directly as the PMD model input. The discussed hysteresis models are implemented in Simulink using (4)–(23), which are expressed in such a form that direct time integration without algebraic loops is enabled.

The ODE models (J-A, GRUCAD, and TLN) are straightforward and easy to implement, whereas the behavioral, equation-free Z-M model requires more effort. The implementation of the Stop model is the most cumbersome of the discussed models, due to the high number of hysterons and discretization of the PMD model.

The data of the evaluated NO SMSSs, experimental setup, and the PMD model is presented in [20]–[22]. The obtained PMD models classify as stiff ODE problems, hence effective calculation is obtained by using MATLAB's variable step solver *ode23tb* (TR-BDF2). The absolute and relative tolerances are set to 10^{-7}.

When comparing the discussed models, the J-A and GRUCAD model have the most challenging parameter identification, whereas the TLN, Z-M, and Stop model can be simply identified directly from standardized quasi-static measurements or alternatively from calculated loops using any other static hysteresis model.

Due to its popularity and wide use, the J-A model is chosen for the reference model and identified first, based on a measured quasi-static major hysteresis loop of $B_{\mathrm{max}} = 1.5\,\mathrm{T}$ using the differential evolution (DE) optimization method [34]. To enable a direct comparison between the applied hysteresis models, the remaining models are identified based on the calculated J-A model major loop. In this way, all the models reproduced identical major (but not minor) static hysteresis loops, except for the GRUCAD model, where also DE is applied. The optimized GRUCAD major loop, hence, deviated slightly from the J-A reference loop.

V. Results

The obtained PMD models are tested for different sinusoidal and distorted excitation waveforms for frequencies up to $f = 200\,\mathrm{Hz}$ and magnetic flux densities up to $B_{\mathrm{max}} = 1.5\,\mathrm{T}$. Different hysteresis models are evaluated by comparing the calculated and measured major and minor dynamic hysteresis loops for the NO steel grade *M400-50A*. In order to provide a comprehensive analysis, both current as well as voltage-driven model versions are evaluated.

The results for dynamic major loops are surprisingly similar for all used models independent from the excitation type when using sinusoidal voltage excitation. Comparing the dynamic ma-

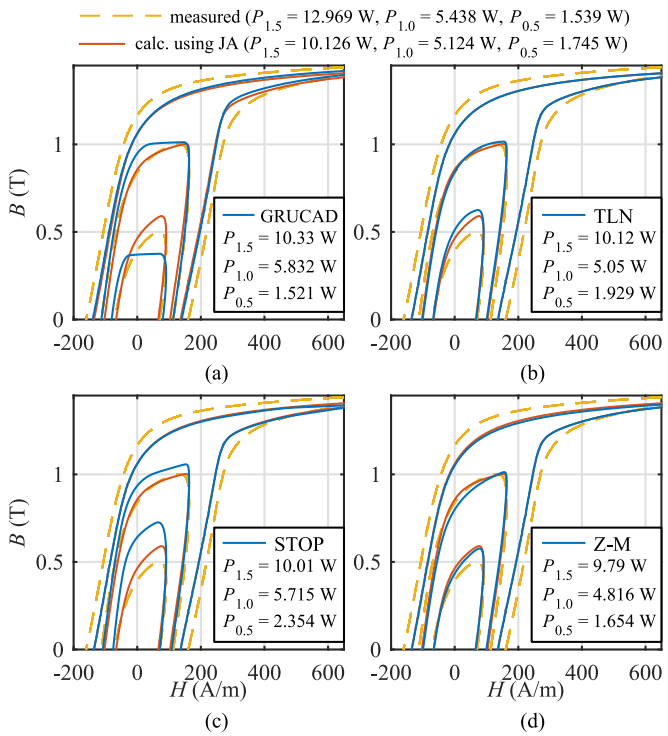

Fig. 1. Comparison of dynamic hysteresis loops using sinusoidal excitation of frequency $f = 200\,\mathrm{Hz}$ using current-driven model version.

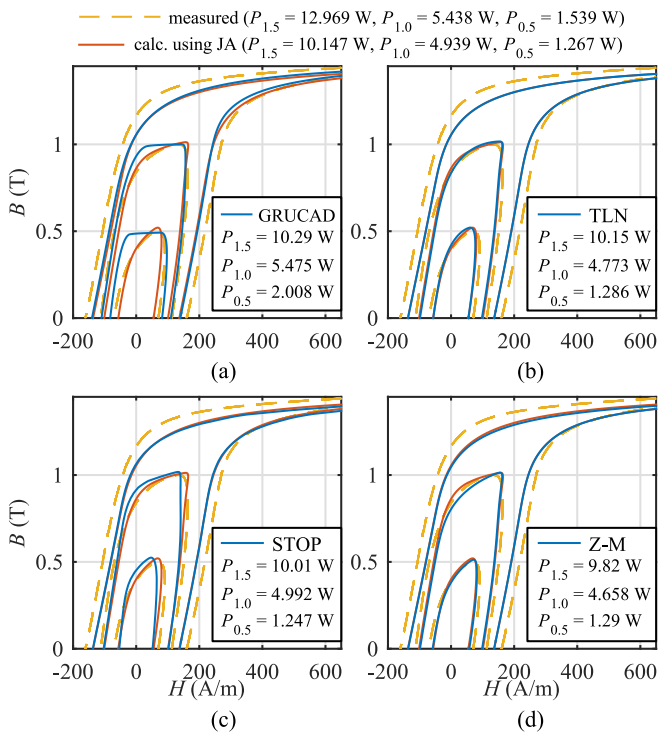

Fig. 2. Comparison of dynamic hysteresis loops using sinusoidal excitation of frequency $f = 200\,\mathrm{Hz}$ using voltage-driven model version.

jor loops at $B_{\max} = 1.5\,\mathrm{T}$ only slight differences between individual models are apparent within the studied magnetic flux density and frequency range [Figs. 1 and 2]. The calculated power losses P support the graphical evaluation, where the deviation of measured power loss is attributed to the lack of viscosity model extension (see Section II). Larger differences between models are obtained when comparing symmetrical minor loops in Figs. 1 and 2; such results are however natural and expected as each hysteresis model has its own internal mechanism to predict inner loops. It is worthwhile to note that the used hysteresis models were identified using only the major loop and were not optimized based on minor loops.

Based on these results, the models are studied subjected to distorted excitation waveforms that generate complex dynamic magnetization curves with off-set minor loops. Such curves are sound candidates to gain further insight of the differences between the used models. First, the sinusoidal excitation waveforms are distorted using harmonics of different order and phase angle [35]. In addition to the fundamental component of frequency $f = 200\,\mathrm{Hz}$ with phase angle $0°$, a fifth harmonic component with phase angle $45°$ is added. The comparison for said excitation case is shown in Fig. 3 for current- and in Fig. 4 for voltage-driven excitation at $B_{\max} = 1.5\,\mathrm{T}$, respectively. Similarly to symmetric major loops there are no significant differences between used models for both excitation cases. Relatively small deviations between magnetization curves appear in the region of the asymmetric minor loop, whereas bigger deviations occur using the current-driven excitation.

Valuable insight is gained into the model peculiarities when using described distorted excitation at lower $B_{\max}$. Figs. 5 and 6 display the comparison of dynamic loops at $B_{\max} = 1.0\,\mathrm{T}$, where significant differences between predicted magnetization curves are obtained. The results show that the best prediction versus measurements is obtained using J-A and TLN models for both excitation cases [see Figs. 5(b) and 6(b)]. The prediction of the Z-M model is of similar accuracy in the voltage-driven case [see Fig. 6(d)], whereas the current-driven version features deviations, in particular, in the asymmetric minor loop region [see Fig. 5(d)]. Predicted magnetization curves of the GRUCAD and Stop models agree equally well with the measurements in the voltage-driven case [see Fig. 6(a) and (c)]. Bigger deviation of the GRUCAD model appear at the minor loop [see Fig. 6(a)]. In contrast to this, the latter two models show significant deviations in the current-driven case [see Fig. 5(a) and (c)], where the almost nonexistent minor loop of the GRUCAD model should be noted [see Fig. 5(a)]. The same conclusions apply when comparing all other evaluated hysteresis models to the reference J-A model.

In addition, important information is gained comparing the magnetization curves of individual models in current [see Fig. 5] and voltage [see Fig. 6] excitation cases. It is natural that the models predict correctly $B_{\max} = 1.0\,\mathrm{T}$ in the voltage-driven case, where H adjusts according to the $H(B)$ relation. In the current-driven case $B_{\max}$ depends on the $B(H)$ relation as H is imposed. It is remarkable that the biggest deviations between excitation cases are obtained using the GRUCAD and Stop models. These results suggest that these two models exhibit limitations and/or are not identified sufficiently accurate in this paper for predicting dynamic magnetization curves with reversal points at lower $B_{\max}$. Observed deviations of the

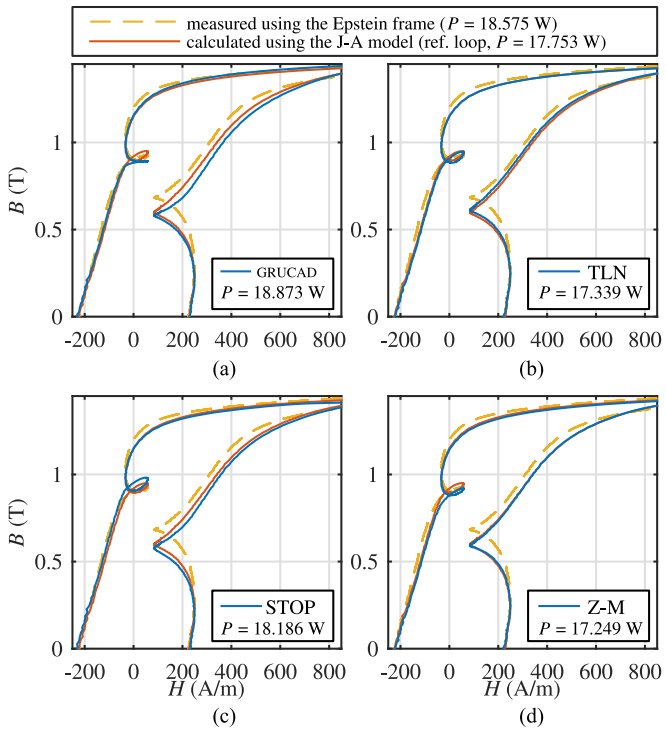

Fig. 3. Comparison of dynamic hysteresis loops for distorted harmonic excitation at $B_{\max} = 1.5\,\mathrm{T}$ using current-driven excitation.

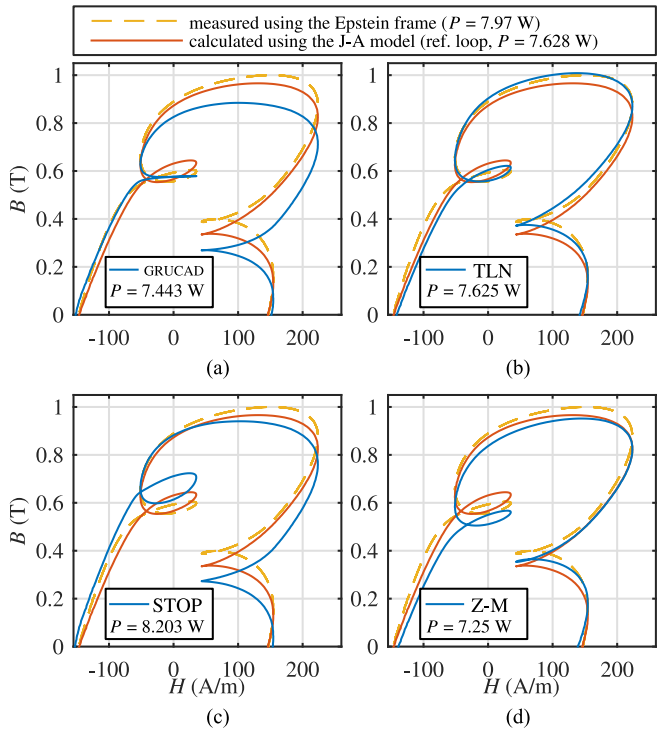

Fig. 5. Comparison of dynamic hysteresis loops for distorted harmonic excitation at $B_{\max} = 1.0\,\mathrm{T}$ using current-driven excitation.

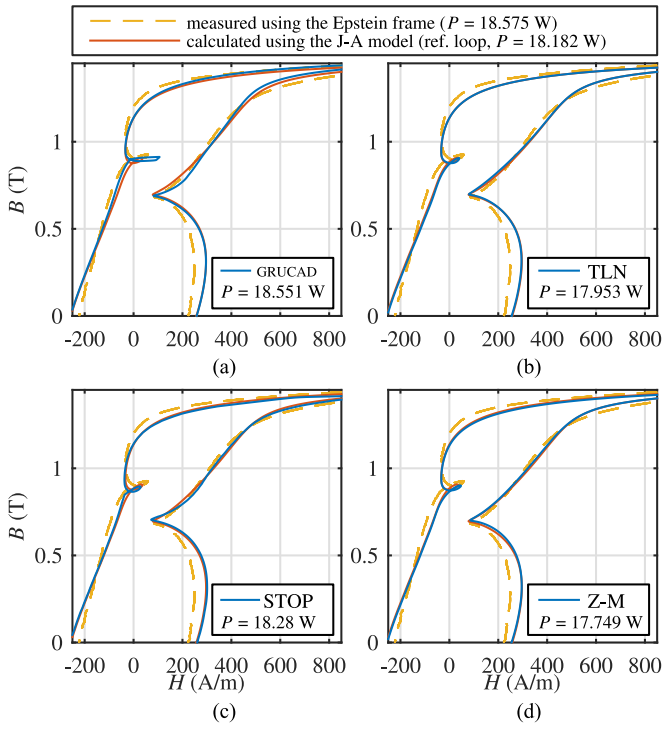

Fig. 4. Comparison of dynamic hysteresis loops for distorted harmonic excitation at $B_{\max} = 1.5\,\mathrm{T}$ using voltage-driven excitation.

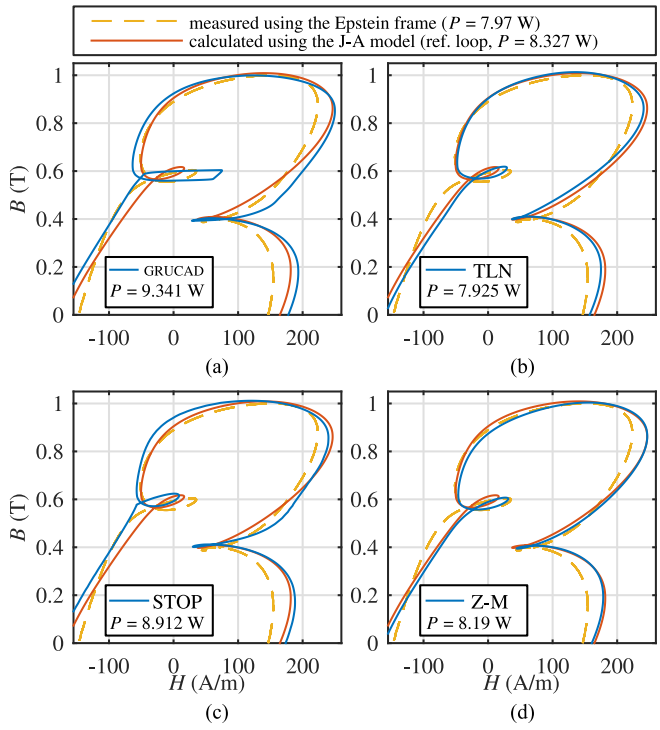

Fig. 6. Comparison of dynamic hysteresis loops for distorted harmonic excitation at $B_{\max} = 1.0\,\mathrm{T}$ using voltage-driven excitation.

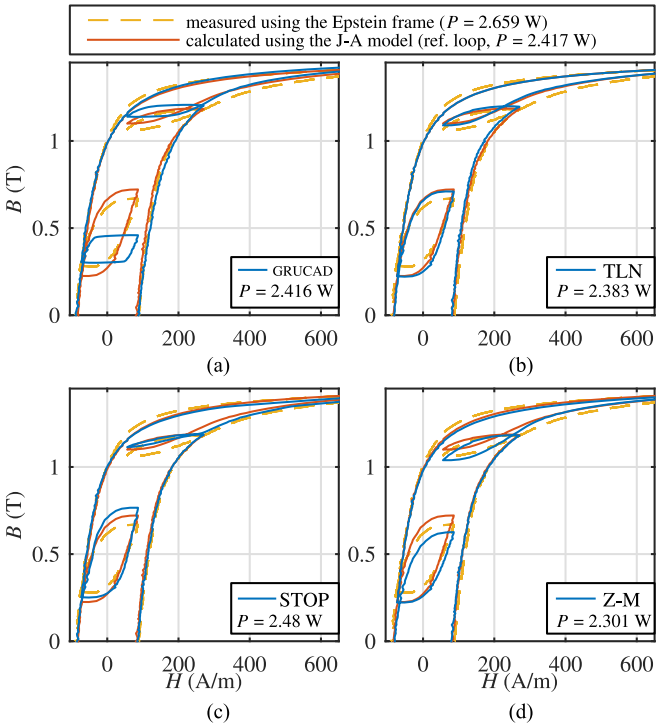

Fig. 7. Comparison of dynamic hysteresis loops for PWM-like excitation of frequency $f = 50\,\mathrm{Hz}$ and $B_{\max} = 1.5\,\mathrm{T}$ using current-driven excitation.

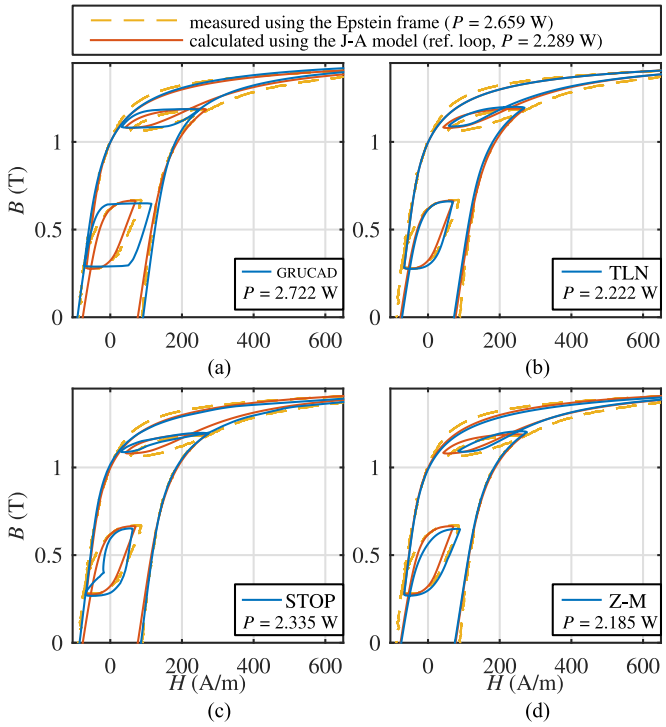

Fig. 8. Comparison of dynamic hysteresis loops for PWM-like excitation of frequency $f = 50\,\mathrm{Hz}$ and $B_{\max} = 1.5\,\mathrm{T}$ using voltage-driven excitation.

GRUCAD model show minor hysteresis loops of somewhat rectangular shape [see Figs. 1(a)–6(a)] which can be assigned to inaccurate identification of the hysteresis part of the model (see Section III-B, parameters H_{h}, λ_{h}, and a_{h}). To achieve better results, the hysteresis part of the GRUCAD model needs more complex parameter identification that includes sets of measured minor loops.

Further insight regarding the deviations of asymmetrical minor loops and complex magnetizations is obtained by applying PWM-like excitation voltages (see [22]). In this way, the applied models are evaluated under rapid changes of the excitation voltage and current that are typical in magnetic components of modern PWM-fed machines. The comparisons for such cases are shown in Figs. 7–10 for $B_{\max} = 1.5\,\mathrm{T}$ and $B_{\max} = 1.0\,\mathrm{T}$, respectively. The results show that the differences between models under such excitations increase further in comparison to smoother excitation waveforms.

When comparing the models under complex magnetizations, the determination of the best fit between calculated curves and measurements is very challenging; to evaluate the goodness of fit, in general, graphical and numerical measures can be used. The simpler and often more adequate approach is using graphical measures that easily display a wide range of relationships between magnetization curves of different models. In contrast to the graphical approach, various numerical measures should be used with care, as they often compress to much information into a single number and can quickly become useless or misleading. For example, quantitative metrics such as losses cannot

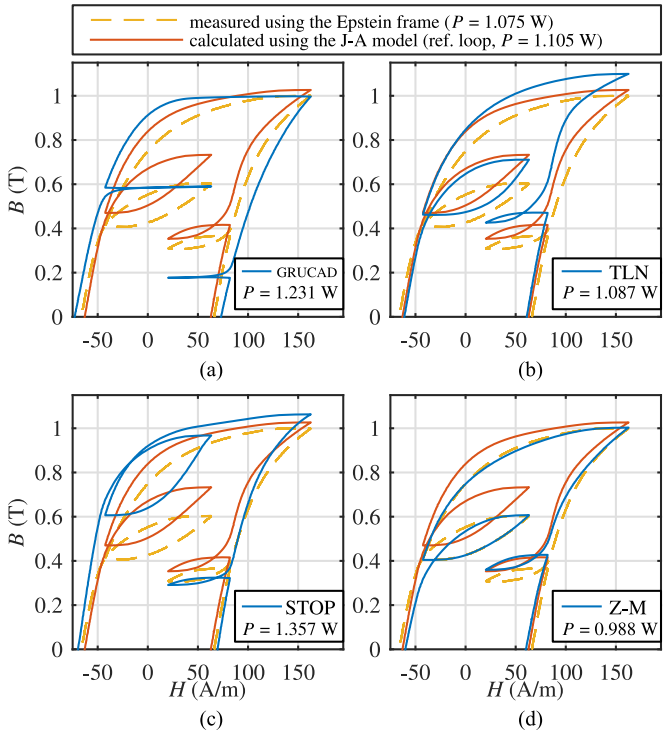

Fig. 9. Comparison of dynamic hysteresis loops for PWM-like excitation of frequency $f = 50\,\mathrm{Hz}$ and $B_{\max} = 1.0\,\mathrm{T}$ using current-driven excitation.

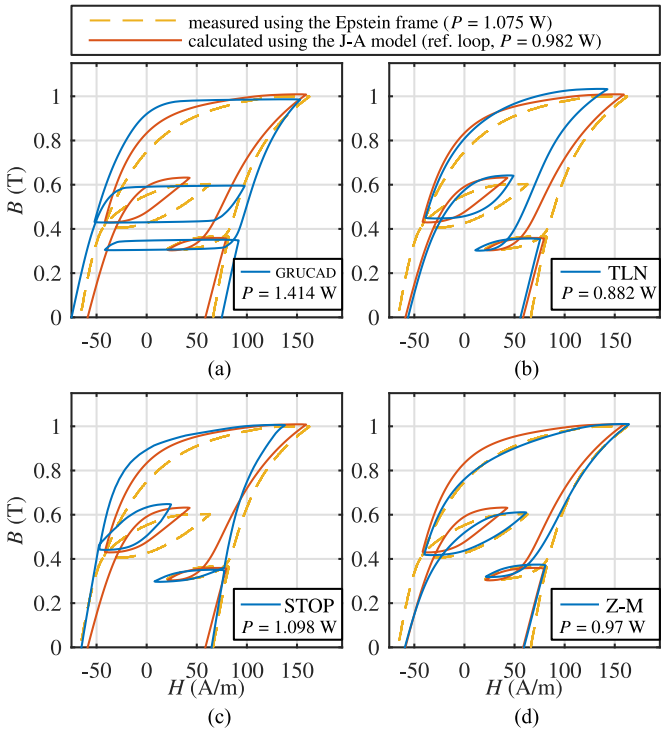

Fig. 10. Comparison of dynamic hysteresis loops for PWM-like excitation of frequency $f = 50\,\mathrm{Hz}$ and $B_{\max} = 1.0\,\mathrm{T}$ using voltage-driven excitation.

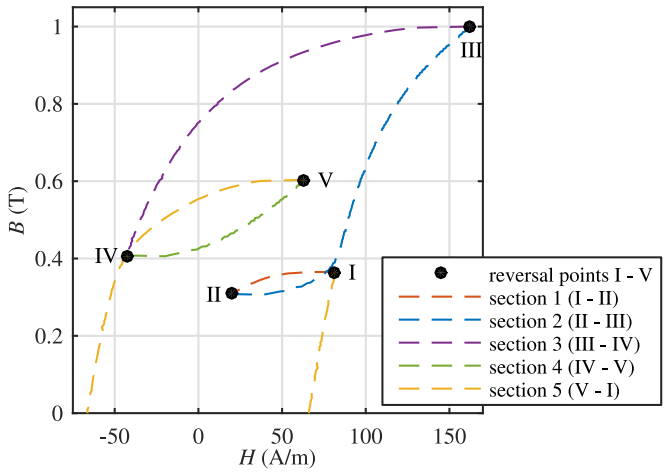

Fig. 11. Division of the dynamic hysteresis loop into five sections.

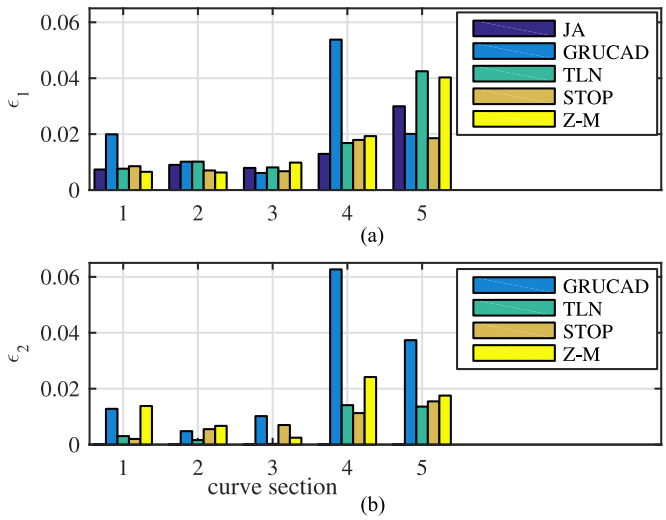

Fig. 12. Calculated NRMS errors ϵ_1 (a) and ϵ_2 (b) of the dynamic loop sections for PWM-like excitation of frequency $f = 50\,\mathrm{Hz}$ and $B_{\max} = 1.5\,\mathrm{T}$ (see Fig. 7) using different hysteresis models under current-driven excitation.

show where the deviation of different magnetization curves is the biggest, as can be seen from the presented results. Statistical measures such as the normalized root-mean square (NRMS) deviation can be more adequate, however, great care is advised. For example, when considering complex dynamic loops with many different magnetization curves and minor loops, individual sections of different curves should be evaluated separately, which leads to a complex analysis.

In addition to the graphical evaluation of the representation, the shape of the hysteresis loop by the different hysteresis models (see Figs. 7–10), numerical measures to evaluate the accuracy quantitatively are applied. In order to elaborate the goodness of fit of individual models, the magnetization cycle caused by the PWM-like excitation is divided into five sections (magnetization trajectories) which are separated by the five reversal points, as shown in Fig. 11. For these individual curve sections, the NRMS errors are calculated using

$$\epsilon = \sqrt{\frac{1}{n}\sum_{t=1}^{n}(\Delta y_t)^2} \tag{24}$$

where two different methods to evaluate the deviation Δy_t are applied. In the current-driven case, the imposed surface H is identical when using all the models, hence, Δy_t is determined directly from the relative deviation of B by (25)

$$\Delta y_t = \frac{(B_{\mathrm{ref}} - B_{\mathrm{calc}})}{\Delta B_{\mathrm{ref}}} \tag{25}$$

where a reference magnetic flux density B_{ref} is compared to the calculated magnetic field density B_{calc} in individual time steps and divided by the range of B_{ref}, i.e., $\Delta B_{\mathrm{ref}} = 2B_{\max}$. For B_{ref} either the measured values [$B_{\mathrm{ref}} \equiv B_{\mathrm{meas}}$, Figs. 12(a) and 14(a)] or calculated values using the J-A model [$B_{\mathrm{ref}} \equiv B_{J-A}$, Figs. 12(b) and 14(b)] are used instead, where NRMS deviations ϵ_1 and ϵ_2 are obtained, respectively. The results for the five different hysteresis models related to the dynamical hysteresis loops shown in Figs. 7 and 9 are given in Figs. 12 and 14. Significant differences are apparent depending on the considered section.

However, when analyzing the voltage excitation case, the NRMS deviation calculation using (25) is not adequate. Due to additional winding (3) B is not imposed, but rather u_{p}. Consequently not only predicted H of different models deviates in individual time steps, but also B. This leads to significantly different reversal points in the H-B plane when different hysteresis models are used, e.g., see Fig. 10. Hence, the distances between points in the H-B plane at the same time step represent a more adequate basis to calculate NRMS deviations. Distances

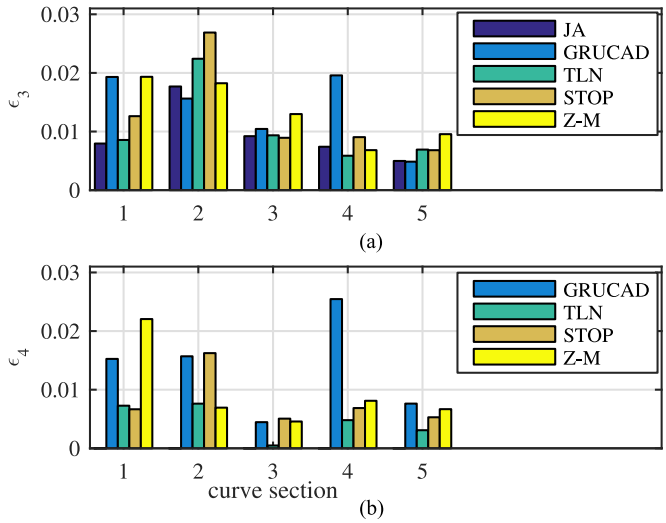

Fig. 13. Calculated NRMS errors ϵ_3 (a) and ϵ_4 (b) of the dynamic loop sections for PWM-like excitation of frequency $f = 50\,\mathrm{Hz}$ and $B_{\max} = 1.5\,\mathrm{T}$ (see Fig. 8) using different hysteresis models under voltage-driven excitation.

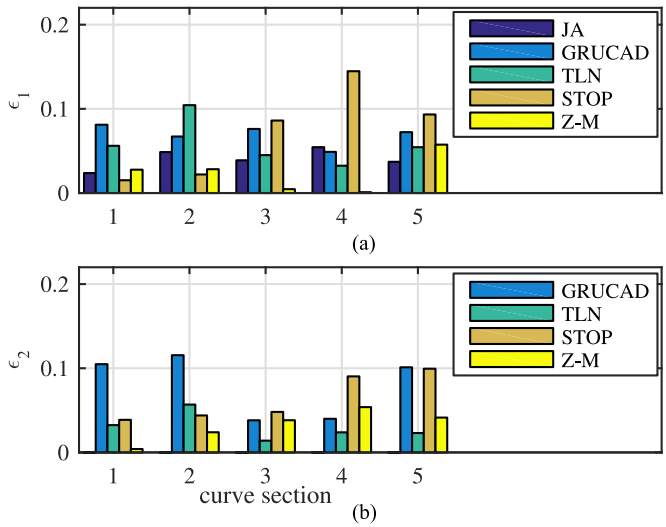

Fig. 14. Calculated NRMS errors ϵ_1 (a) and ϵ_2 (b) of the dynamic loop sections for PWM-like excitation of frequency $f = 50\,\mathrm{Hz}$ and $B_{\max} = 1.0\,\mathrm{T}$ (see Fig. 9) using different hysteresis models under current-driven excitation.

at the individual time steps are calculated by

$$\Delta y_t = \sqrt{\left(\frac{B_{\mathrm{ref}} - B_{\mathrm{calc}}}{\Delta B_{\mathrm{ref}}}\right)^2 + \left(\frac{H_{\mathrm{ref}} - H_{\mathrm{calc}}}{\Delta H_{\mathrm{ref}}}\right)^2} \tag{26}$$

where ΔH_{ref} is the range of H_{ref}, i.e., $\Delta H_{\mathrm{ref}} = 2H_{\max}$.

Similar to the current-driven case, also in this case two different references are used, either measured ($B_{\mathrm{ref}} \equiv B_{\mathrm{meas}}$) or calculated values using the reference J-A model ($B_{\mathrm{ref}} \equiv B_{J-A}$), yielding ϵ_3 and ϵ_4, respectively. The results for the five different hysteresis models related to the dynamical hysteresis loops shown in Figs. 8 and 10 are given in Figs. 13 and 15.

Using graphical evaluation in Figs. 7–10, it could be argued that the best overall fit (taking into account both excitation cases) versus measurements is obtained by using the Z-M hysteresis

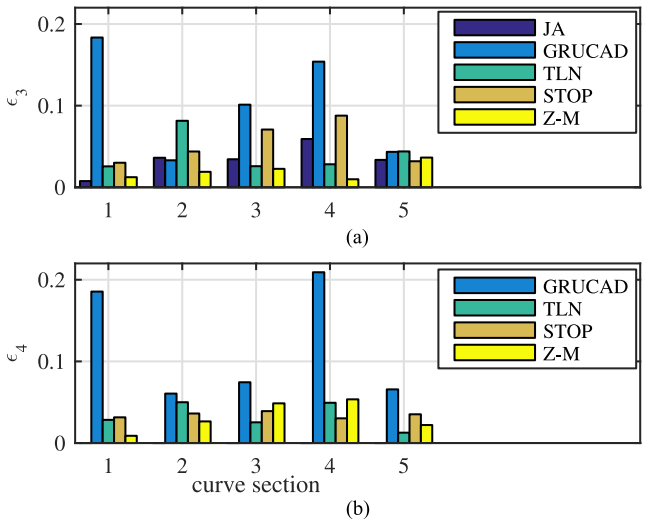

Fig. 15. Calculated NRMS errors ϵ_3 (a) and ϵ_4 (b) of the dynamic loop sections for PWM-like excitation of frequency $f = 50\,\mathrm{Hz}$ and $B_{\max} = 1.0\,\mathrm{T}$ (see Fig. 10) using different hysteresis models under voltage-driven excitation.

model, despite the fact that this model is not identified directly from the measured static loop. This conclusion is supported by the calculated NRMS deviations, where the Z-M outperforms other models in most sections, in particular at lower $B_{\max}$ [see Figs. 14(a)–15(a)]. From results in Fig. 13(a), it could be argued that the Z-M is not as accurate as the other models at $B_{\max} = 1.5\,\mathrm{T}$ in the voltage-driven case. However, as noted before, at higher $B_{\max}$ the models perform very similar and NRMS deviations between them are mostly lower than 1%. The results show that the only weak section of the Z-M model is section V which becomes visible also using graphical measures.

Furthermore, when comparing all other models to the reference J-A model, the best overall fit represents the TLN model. This can be concluded using graphical measures (see Figs. 7–10) and is supported by the calculated NRMS deviations [see Figs. 12(b)–15(b)]. The same conclusions were also drawn from the analysis using pure and distorted sinusoidal excitations [see Figs. 1(b)–6(b)]. Consequently, it can be concluded that this model internal mechanisms are surprisingly similar to the J-A model. The largest drawback of the TLN model is, however, section II (when the ascending branch is approaching the $B_{\max}$), where almost all other models predict better results. The results of the Stop and Z-M are also comparable, where each has its advantages or drawbacks in different sections. The difference of the off-set minor loops predicted by the Stop model in the current- and voltage-driven cases that was observed using distorted sinusoidal excitation [see Figs. 3(c)–6(c)], is observed also in Figs. 9(c) and 10(c).

The worst results versus measurements and the reference J-A model are obtained using the GRUCAD model. This model performs decent when the magnetization curve follows outer curves of the dynamic hysteresis. In contrast to this, the PWM excitation case supports the previous conclusions that the minor loops are far off. These loops are determined from the hysteresis part of the model (see Section III-B), where poor results shows inadequate identification of these parameters. Consequently, it

can be concluded that the identification procedure of the GRUCAD model parameters is more challenging compared to the J-A model. For a more adequate identification not only measured major loops are sufficient, but also minor loops are needed.

Looking closer at the individual curve sections, some other limitations of individual models are observed: using the J-A, TLN, and partly Z-M models, the minor loops are not closed correctly [see Figs. 9(b), (d) and 10(b), (d) and]. In order to avoid nonclosure of minor loops due to too high magnetization rates in J-A, [36] proposed a semiphysical methodology that limits the variation rate by modifying the k and c parameter (4) of the model. However, this approach leads to additional parameter identification work based on extensive measurements.

Another numerical aspect to evaluate is the computational performance of the approach when different hysteresis models are applied. In general, it is very hard to determine objective computation times as they depend on many variables and deviate significantly under different conditions. Hence, the exact computational efforts are not studied in this paper.

In general, the TLN model outperformed all other models due to its simplicity. The J-A model follows in this respect. The GRUCAD model is close to the J-A model with its results, where the computation times, when these two models are applied, amounted for approximately two times compared to the TLN model. When the Z-M model is applied the computational performance is significantly decreased when compared to the ODE hysteresis models due to its algebraic structure. The worst performance is obtained when the Stop model is applied. The computation times are significantly longer when compared to the Z-M model when a high number of hysterons N_h is used, which is needed for the accurate representation of the static hysteresis. When N_h is lower, the computational performance is increased. However the accuracy in the saturation and minor loop regions significantly decreased. In this paper $N_\mathrm{h} = 60$ hysterons are used.

VI. Conclusion

This paper has compared and analyzed several of the widely used hysteresis models coupled to the PMD model under sinusoidal and arbitrary magnetization waveforms. The importance of considering nonlinear, hysteretic properties when calculating dynamic variables and power loss inside NO SMSSs with nonuniform magnetic fields is pointed out.

The models were directly compared in terms of identification procedure facilities, accuracy, numerical implementation and computational effort, where the J-A model is used as a reference. In this way, the influence of the identification procedure is eliminated.

The application of the coupled approach (lamination model plus static hysteresis model) to arbitrary excitation cases provides detailed insight and a thorough analysis of the discussed hysteresis models. Their ability to predict the dynamic hysteresis loop shape, electromagnetic variables and power loss components under distorted excitation waveforms was examined. Different NRMS errors were evaluated in combination with a thorough graphical analysis.

The presented analysis enables an application-specific selection of the hysteresis model taking account of the actual operation conditions of the electromagnetic energy transducers. Therefore, error-prone and limited engineering approaches commonly used for iron-loss calculation based on a huge amount of measured data can be replaced by the PMD model coupled to the most-suited hysteresis model for considered operation conditions. As a result not only the hysteresis loop shape and magnetization dynamics can be calculated but also the parameter identification effort is reduced to one quasi-static measurement (major hysteresis loop) and the usage of material specific data such as specific electrical conductivity and geometrical data (thickness, ...). Additional measured data allows one to fine tune the hysteresis models.

However, it is apparent that history-independent hysteresis models reach some limitations under strongly distorted excitations such as the PWM-like ones. As the individual models exhibit different limitations to adequately reproduce static hysteresis, the discussed models will be analyzed in the next study when individual models are identified directly from measurements.

The extension to materials with a coarse domain structure, i.e., grain-oriented materials, is possible by introducing a magnetic viscosity to account for the effect of microscopic eddy currents on the movement of domain walls [17].

References

[1] A. Krings, J. Soulard, and O. Wallmark, "PWM influence on the iron losses and characteristics of a slotless permanent-magnet motor with SiFe and NiFe stator cores," *IEEE Trans. Ind. Appl.*, vol. 51, no. 2, pp. 1475–1484, Mar./Apr. 2015.

[2] Z. Gmyrek, A. Boglietti, and A. Cavagnino, "Estimation of iron losses in induction motors: Calculation method, results, and analysis," *IEEE Trans. Ind. Electron.*, vol. 57, no. 1, pp. 161–171, Jan. 2010.

[3] J. Pyrhönen, S. Ruoho, J. Nerg, M. Paju, S. Tuominen, H. Kankaanpää, R. Stern, A. Boglietti, and N. Uzhegov, "Hysteresis losses in sintered NdFeB permanent magnets in rotating electrical machines," *IEEE Trans. Ind. Electron.*, vol. 62, no. 2, pp. 857–865, Feb. 2015.

[4] Q. Yu, B. Bilgin, and A. Emadi, "Loss and efficiency analysis of switched reluctance machines using a new calculation method," *IEEE Trans. Ind. Electron.*, vol. 62, no. 5, pp. 3072–3080, May 2015.

[5] S. Zhu, M. Cheng, J. Dong, and J. Du, "Core loss analysis and calculation of stator permanent-magnet machine considering dc-biased magnetic induction," *IEEE Trans. Ind. Electron.*, vol. 61, no. 10, pp. 5203–5212, Oct. 2014.

[6] N. Soltau, D. Eggers, K. Hameyer, and R. De Doncker, "Iron losses in a medium-frequency transformer operated in a high-power dc-dc converter," *IEEE Trans. Magn.*, vol. 50, no. 2, pp. 953–956, Feb. 2014.

[7] K. Fujisaki and S. Liu, "Magnetic hysteresis curve influenced by power-semiconductor characteristics in pulse-width-modulation inverter," *J. Appl. Phys.*, vol. 115, no. 17, 2014, Art. no. 17A321.

[8] A. Boglietti and A. Cavagnino, "Iron loss prediction with PWM supply: An overview of proposed methods from an engineering application point of view," *Elect. Power Syst. Res.*, vol. 80, no. 9, pp. 1121–1127, 2010.

[9] M. Popescu, D. Ionel, A. Boglietti, A. Cavagnino, C. Cossar, and M. McGilp, "A general model for estimating the laminated steel losses under PWM voltage supply," *IEEE Trans. Ind. Appl.*, vol. 46, no. 4, pp. 1389–1396, Jul./Aug. 2010.

[10] Z. Gmyrek, A. Boglietti, and A. Cavagnino, "Iron loss prediction with PWM supply using low- and high-frequency measurements: analysis and results comparison," *IEEE Trans. Ind. Electron.*, vol. 55, no. 4, pp. 1722–1728, Apr. 2008.

[11] H. Gorginpour, H. Oraee, and E. Abdi, "Calculation of core and stray load losses in brushless doubly fed induction generators," *IEEE Trans. Ind. Electron.*, vol. 61, no. 7, pp. 3167–3177, Jul. 2014.

[12] S. E. Zirka, Y. I. Moroz, P. Marketos, and A. J. Moses, "Comparison of engineering methods of loss prediction in thin ferromagnetic laminations," *J. Magn. Magn. Mater.*, vol. 320, no. 20, pp. 2504–2508, 2008.

[13] S. E. Zirka, Y. I. Moroz, P. Marketos, and A. J. Moses, "Evolution of the loss components in ferromagnetic laminations with induction level and frequency," *J. Magn. Magn. Mater.*, vol. 320, no. 20, pp. 1039–1043, 2008.
[14] S. Zirka, Y. Moroz, R. Harrison, and N. Chiesa, "Inverse hysteresis models for transient simulation," *IEEE Trans. Power Del.*, vol. 29, no. 2, pp. 552–559, Apr. 2014.
[15] S. Zirka, Y. Moroz, P. Marketos, A. Moses, D. Jiles, and T. Matsuo, "Generalization of the classical method for calculating dynamic hysteresis loops in Grain-Oriented electrical steels," *IEEE Trans. Magn.*, vol. 44, no. 9, pp. 2113–2126, Sep. 2008.
[16] F. Henrotte and K. Hameyer, "A dynamical vector hysteresis model based on an energy approach," *IEEE Trans. Magn.*, vol. 42, no. 4, pp. 899–902, Apr. 2006.
[17] S. Zirka, Y. Moroz, S. Steentjes, K. Hameyer, K. Chwastek, S. Zurek, and R. Harrison, "Dynamic magnetization models for soft ferromagnetic materials with coarse and fine domain structures," *J. Magn. Magn. Mater.*, vol. 394, pp. 229–236, 2015.
[18] S. E. Zirka, Y. I. Moroz, A. J. Moses, and C. M. Arturi, "Static and dynamic hysteresis models for studying transformer transients," *IEEE Trans. Power Del.*, vol. 26, no. 4, pp. 2352–2362, Oct. 2011.
[19] M. Petrun, S. Steentjes, K. Hameyer, and D. Dolinar, "One-dimensional lamination models for calculating the magnetization dynamics in non-oriented soft magnetic steel," *IEEE Trans. Magn.*, vol. 52, no. 3, 2015, Art. no. 7002904.
[20] M. Petrun, V. Podlogar, S. Steentjes, K. Hameyer, and D. Dolinar, "A parametric magneto-dynamic model of soft magnetic steel sheets," *IEEE Trans. Magn.*, vol. 50, no. 4, pp. 1–4, Apr. 2014.
[21] M. Petrun, V. Podlogar, S. Steentjes, K. Hameyer, and D. Dolinar, "Power loss calculation using the parametric magneto-dynamic model of soft magnetic steel sheets," *IEEE Trans. Magn.*, vol. 50, no. 11, pp. 1–4, Nov. 2014.
[22] M. Petrun, S. Steentjes, K. Hameyer, and D. Dolinar, "Magnetization dynamics and power loss calculation in NO soft magnetic steel sheets under arbitrary excitation," *IEEE Trans. Magn.*, vol. 51, no. 1, pp. 1–4, Jan. 2015.
[23] S. Bi, F. Wolf, R. Lerch, and A. Sutor, "An inverted preisach model with analytical weight function and its numerical discrete formulation," *IEEE Trans. Magn.*, vol. 50, no. 11, pp. 1–4, Nov. 2014.
[24] T. Matsuo and M. Shimasaki, "Two types of isotropic vector play models and their rotational hysteresis losses," *IEEE Trans. Magn.*, vol. 44, no. 6, pp. 898–901, Jun. 2008.
[25] T. Matsuo, D. Shimode, Y. Terada, and M. Shimasaki, "Application of stop and play models to the representation of magnetic characteristics of silicon steel sheet," *IEEE Trans. Magn.*, vol. 39, no. 3, pp. 1361–1364, May 2003.
[26] A. Bergqvist, "Magnetic vector hysteresis model with dry friction-like pinning," *Physica B: Condensed Matter*, vol. 233, no. 4, pp. 342–347, 1997.
[27] S. Steentjes, F. Henrotte, C. Geuzaine, and K. Hameyer, "A dynamical energy-based hysteresis model for iron loss calculation in laminated cores," *Int. J. Numerical Model., Electron. Netw. Devices Fields*, vol. 27, no. 3, pp. 433–443, 2014.
[28] H. Hauser, "Energetic model of ferromagnetic hysteresis: Isotropic magnetization," *J. Appl. Phys.*, vol. 96, no. 5, pp. 2753–2767, 2004.
[29] P. Koltermann, L. Righi, J. Bastos, R. Carlson, N. Sadowski, and N. Batistela, "A modified Jiles method for hysteresis computation including minor loops," *Phy. B, Condensed Matter*, vol. 275, no. 1–3, pp. 233–237, 2000.
[30] D. Jiles and D. Atherton, "Theory of ferromagnetic hysteresis," *J. Magn. Magn. Mater.*, vol. 61, no. 1–2, pp. 48–60, 1986.
[31] B. Vaseghi, D. Mathekga, S. Rahman, and A. Knight, "Parameter optimization and study of inverse J-A hysteresis model," *IEEE Trans. Magn.*, vol. 49, no. 5, pp. 1637–1640, May 2013.
[32] S. Zirka, Y. Moroz, R. Harrison, and K. Chwastek, "On physical aspects of the Jiles-Atherton hysteresis models," *J. Appl. Phys.*, vol. 112, no. 4, 2012, Art. no. 043916.
[33] J. Tellinen, "A simple scalar model for magnetic hysteresis," *IEEE Trans. Magn.*, vol. 34, no. 4, pp. 2200–2206, Jul. 1998.
[34] M. Zaman and M. Matin, "Optimization of Jiles-Atherton hysteresis model parameters using taguchis method," *IEEE Trans. Magn.*, vol. 51, no. 5, 2014, Art. no. 7301004.
[35] T. Kefalas and A. Kladas, "Harmonic impact on distribution transformer No-Load loss," *IEEE Trans. Ind. Electron.*, vol. 57, no. 1, pp. 193–200, Jan. 2010.
[36] A. Benabou, J. Leite, S. Clenet, C. Simao, and N. Sadowski, "Minor loops modelling with a modified Jiles-Atherton model and comparison with the Preisach model," *J. Magn. Magn. Mater.*, vol. 320, no. 20, pp. e1034–e1038, 2008.

Simon Steentjes received the Diploma degree in electrical engineering from RWTH Aachen University, Aachen, Germany, in November 2011.

He has been working as a Research Associate at the Institute of Electrical Machines, RWTH Aachen University, since December 2011. His research interests include hard- and soft-magnetic material modeling on the micro and macroscopic scale, iron loss calculation, effects of material processing, magnetic forces, and mathematical methods.

Kay Hameyer (M'96–SM'99) received the M.Sc. degree in electrical engineering from the University of Hanover, Hanover, Germany, in 1986, and the Ph.D. degree from the University of Technology Berlin, Berlin, Germany, in 1992, for work on permanent-magnet excited machines.

After his university studies, he worked with Robert Bosch GmbH, Stuttgart, Germany, as a Design Engineer for permanent-magnet servo motors. From 1988 to 1993, he was a Member of Staff at the University of Technology Berlin. From 1996 to 2004, he was a Full Professor of numerical field computations and electrical machines, Katholieke Universiteit Leuven (KU Leuven), Leuven, Belgium. Since 2004, he has been a Full Professor and the Director of the Institute of Electrical Machines, RWTH Aachen University, Aachen, Germany. His research interests include all aspects of the design, control, and manufacturing of electrical machines and the associated numerical simulations. The characterization and modeling of hard- and soft-magnetic materials is another focus of his work. He has authored/coauthored more than 250 journal publications, more than 500 international conference publications, and 4 books.

Dr. Hameyer has been a Member of the German VDE since 2004 and, since 2002, a Fellow of the Institution of Engineering and Technology, U.K.

Drago Dolinar (M'81) received the B.Sc. E.E., M.Sc., and Ph.D. degrees in electrical engineering from the University of Maribor, Maribor, Slovenia, in 1978, 1980 and 1985, respectively.

Since 1981, he has been with the Faculty of Electrical Engineering and Computer Science, University of Maribor, where he is currently a Professor. His current research interests include modeling and control of electrical machines.

Dr. Dolinar is a Member of the Institution of Engineering and Technology, U.K., ICS, the Conseil International des Grands Reseaux Electriques, and the Slovenian Simulation Society.

Martin Petrun (M'11) received the BSc. E.E and Ph.D. degrees in electrical engineering from the University of Maribor, Maribor, Slovenia, in 2010 and 2014, respectively.

He is currently a Researcher and an Assistant Professor at the University of Maribor. His current research interests include modeling of dynamic phenomena inside soft-magnetic materials as well as modeling and control of electrical and electromechanical converters and power electronics.